



A study on the quality of GNSS signals for extracting the sea level height and tidal frequencies utilizing the GNSS-IR approach

Sara Gholamrezaee¹ · Mohammad Bagherbandi^{2,3} · Kamal Parvazi¹ · Saeed Farzaneh¹

Received: 20 August 2022 / Accepted: 4 February 2023 / Published online: 15 February 2023
© The Author(s), under exclusive licence to Springer-Verlag GmbH Germany, part of Springer Nature 2023

Abstract

Coastal global navigation satellite system (GNSS) stations equipped with a standard geodetic receiver and antenna enable water level measurement using the GNSS interferometry reflectometry (GNSS-IR) technique. By using GNSS-IR, the vertical distance between the antenna and the reflector surface (e.g., water surface) can be obtained in the vertical (height) reference frame. In this study, the signal-to-noise ratio (SNR) data from four selected stations over three months are used for this purpose. We determined the predominant multipath frequency in SNR data that is obtained using Lomb–Scargle periodogram (LSP) method. The obtained sea surface heights (SSH) are assessed using tide gauge observations regarding accuracy and correlation coefficients. In this study, we investigated daily and hourly GNSS observations and used single frequencies of GPS (L1, L2 and L5), GLONASS (L1 and L2), Galileo (L1, L5, L6, L7 and L8), and BeiDou (L2 and L7) signals to estimate the SSH. The results show that the optimal signals for extracting the SSH are the L1 signal for the GPS, Galileo, and GLONASS systems and the L2 signal for the BeiDou system. The accuracy and correlation parameters for the optimal GPS signal in the daily mode are 2 cm and 0.87, respectively. The same parameters for the optimal GLONASS signal are 4 cm and 0.91. However, the obtained accuracy and correlation coefficients using the best Galileo and BeiDou signals are reduced, i.e., 4 cm and 0.88 using Galileo and 12 cm and 0.52 by employing the Galileo signals, respectively. Our results also show that the GPS L1 signal is more consistent with the tide gauge data. In the following, using the time series derived from the L1 signal and tide gauge readings, the tidal frequencies are extracted and compared using the Least Square Harmonic Estimation (LS-HE) approach. The findings demonstrate that 145 significant tidal frequencies can be extracted using the GNSS-IR time series. The existence of an acceptable correlation between the tidal frequencies of the GNSS-IR and the tide gauge time series indicates the usefulness of the GNSS-IR time series for tide studies. From our results, we can conclude that the GNSS-IR technique can be applied in coastal locations alongside tide gauge measurements for a variety of purposes.

Keywords GNSS interferometry reflectometry · Sea level height · Tide-gauge · Frequency analysis · LS-HE · Remote sensing

✉ Saeed Farzaneh
farzaneh@ut.ac.ir

¹ School of Surveying and Geospatial Engineering, College of Engineering, University of Tehran, North Kargar Street, Tehran 1439957131, Iran

² Faculty of Engineering and Sustainable Development, University of Gävle, Gävle, Sweden

³ Division of Geodesy and Satellite Positioning, Royal Institute of Technology (KTH), Stockholm, Sweden

Introduction

Tides in open water, e.g., seas and oceans, have long been observed by coastal inhabitants as a periodic phenomenon that changes the coastlines. Oceanographers have studied these water level changes to better understand physical processes within the earth's system and enhance their spatial and temporal predictions (Cohen et al. 1997). Accurate and effective monitoring of water level variations and their effects on societal development has been of the utmost importance since coastal regions are crucial to global economic operations (Cohen et al. 1997; Feng et al. 2013).

The installation of tide gauge stations along the coasts allows for the analysis of sea surface changes as a component

of both global and regional monitoring networks (Olivieri and Spada 2016; Pajak and Kowalczyk 2019). However, observations from these stations are used not only to measure sea surface changes but also to monitor long-term changes due to vertical land motions (Vestøl 2006; Larson et al. 2013). Tide-gauge stations measure the oscillations of water levels concerning the surrounding land. A precise vertical land motion model is required because the tide-gauge station motions lead to inaccurate sea level observations. Therefore, it is also necessary to monitor sea-level changes using alternative modern technologies. For many years, satellite altimetry has been an effective method for tracking sea-level changes by providing highly accurate estimates in deep, calm sea and ocean areas (Vignudelli et al. 2019; Farzaneh and Parvazi 2020; Peng et al. 2019). The accuracy of altimetry around the coastlines considerably decreases, mainly because of the imperfect reflection of the radar waveforms in the shallow areas and the radar signal reflections from land (Vignudelli et al. 2011), which requires unique treatments.

The global navigation satellite system (GNSS) is primarily designed for positioning and navigation applications (Castagnetti et al. 2009). Previous research has shown that GNSS-IR, which exploits the interference between direct and reflected GNSS signals at the antenna site, can also be used to estimate changes in sea level (Benton and Mitchell 2011). Since its introduction in 1993, this technique has been utilized to get sea surface height (SSH) on various terrestrial and aerial platforms (Martin-Neira 1993; Zhang et al. 2019). The GNSS-IR sea-level time series is directly taken from the water surface, unlike traditional tide gauges placed in certain areas to lessen the impact of sea waves on the signal. In order to measure the height of the water surface for areas that are far away from the GNSS station, the height of the antenna is considered an effective parameter in the GNSS-IR technique (Roussel et al. 2015). The common practice to retrieve monthly and yearly SSH changes is to process the signal-to-noise ratio (SNR) provided by GNSS receivers, as demonstrated by Roussel et al. (2015) and Larson et al. (2013).

Strandberg et al. (2016) combined GPS and GLONASS observations to improve SSH estimations, from which an acceptable root mean square error (RMSE) of 1.8 cm was achieved after evaluation against the observations of a pressure mareograph. Previous studies have shown that the accuracy of GNSS-R results depends on the quality control applied in the observation analysis. Among these cases, we can mention the conditions applied to the elevation angle of the satellite. In fact, by considering a low elevation angle, useful observations can be obtained in retrieving the height from the surface. The dynamic correction of the reflection plate also plays an effective role in improving the quality of the results. This correction plays an important role in eliminating errors caused by dynamic changes to the reflective

surface (Larson et al. 2017). Larson et al. (2013) applied ordinary geodetic receivers to monitor SSH. The observed SSH data from nearby and in situ tidal gauges were compared to the estimated sea level acquired from geodetic receivers. They analyzed their results at Onsala Space Observatory in Sweden and Friday Harbor in the USA. The RMSE of 5 cm was estimated for Onsala and 10 cm for Friday Harbor. A correlation coefficient of 0.97 was obtained between the GNSS-IR derived SSH and in-situ observations of both stations. In another study, the SNR observations were analyzed by Löfgren et al (2014) at five GPS stations in GTGU in Onsala, Sweden; SC02 in Friday Harbor, USA; BRST in Brest, France; BUR2 in Burnie, Australia; and OHI3 in O'Higgins, Antarctica. By comparing the time series obtained from GNSS-IR with the time series obtained from tide-gauge stations, they found correlation coefficients between 0.89 and 0.99. The RMSE differences are on the order of 6.2 cm for low tidal range (up to 165 cm) and 43 cm for high tidal range (up to 772 cm). An analysis of (10-year) GPS observations was presented by Larson et al. (2017), who applied dynamic corrections for surface reflection and elevation angle refraction. Their results indicated an RMSE of 12 cm between the tide-gauge and GNSS-IR data.

Today, it is possible to send many signals from each satellite due to the developments in navigation satellite systems and the increase in the number of satellites in these systems. In this study, due to the change in data quality (SNR) associated with each signal, sea surface change estimation has been studied using the GNSS-IR approach. In the first step, the time series generated from the signals of GPS, GLO-NASS, Galileo, and BeiDou systems are compared with the tide gauge measurements nearby the GNSS stations. For the production of these time series, observations of L1, L2, and L5 signals for the GPS system, L1 and L2 signals for the GLONASS system, L1, L2, L5, L6, L7, and L8 signals for the Galileo system, and L1 and L2 signals for the BeiDou system are used. Then the frequency analysis is examined according to the selection of the most appropriate signal and the use of time series obtained from that signal. There are many methods to extract frequencies, and in this research, we use the univariate least squares harmonic analysis method. Finally, the frequencies obtained from the GNSS-IR time series are compared with those obtained from the tide gauge time series to study different tidal components. The tidal frequencies acquired from the GNSS-IR time series and the tide gauge show a reasonable agreement, which confirms the high accuracy of the GNSS-IR time series for extracting the tidal frequencies.

The following first introduces the study area, the data, and information on the tide-gauge and GNSS stations used in this study. Then it describes the principles of the GNSS-IR technique, Lomb-Scargle spectral analysis, and the least square harmonic estimation method. In addition, the main

results of GNSS-IR are presented. Finally, conclusions and recommendations for future studies are presented.

Data and study area

In this study, the sea surface changes have been obtained using the GNSS data from six stations: GTGU in Sweden, MERS in Turkey, MCHN in Canada, AT01 in the USA, MARS in France, and TGDE in Norway. The reason for choosing these stations is their proximity to the tide gauge,

the possibility of receiving multi-GNSS signals and having a long data time to extract tidal frequencies. Each GNSS receiver measures different signals, including GPS, GLO-NASS, Galileo, and BeiDou. Figures 1 and 2 show the geographical location and image of the GNSS stations. Additional information about the stations is presented in Table S1 (presented in supplementary materials).

Tide gauge data is used as the primary ground data to evaluate the performance of the proposed method (i.e., GNSS-IR). This study selected the closest coastal tide gauge to each GNSS station, as shown in Table S2 (presented in supplementary materials).

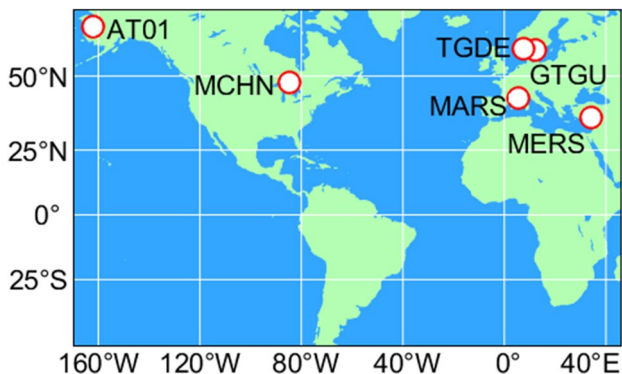


Fig. 1 Geographical location of the GNSS stations used in this study

Basics water level measurement using GNSS-IR method

Installing a geodetic GNSS receiver in the coastal areas and applying the GNSS-IR method will allow the water level to be measured. Using SNR observations, it is possible to measure the height difference between the antenna and the reflector surface. The SNR observations are actually a measure of the strength of the signal received by the antenna. This parameter primarily indicates the direct signal power (line of sight) but can also be affected secondarily by the reflected signal power. The SNR observations can fluctuate

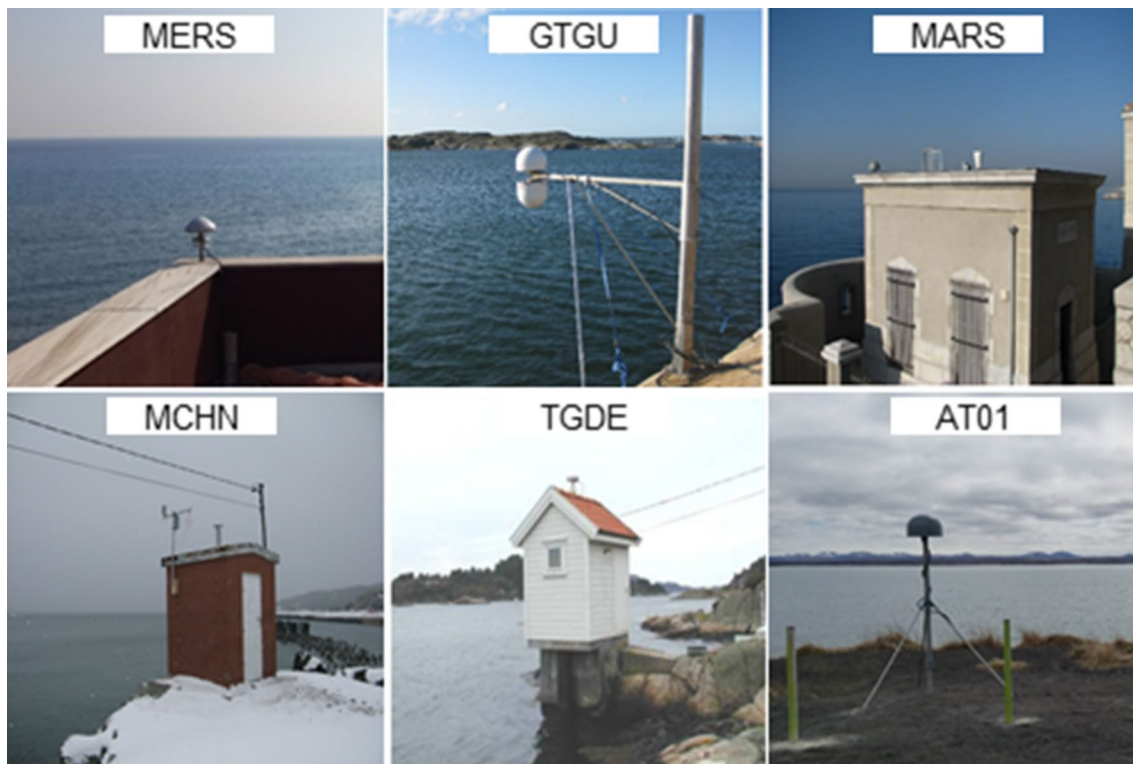


Fig. 2 Overview of the GNSS sites (<https://www.sonel.org/>)

due to interference between direct and reflected signals at low elevation angles. For example, the SNR changes of the GPS satellite number 32 for the station MARS on the first day of 2018 are presented in Fig. 3. The height parameter of the GNSS antenna to the desired level (here, sea level) can be obtained using the interference between direct and reverse signals (obtained by SNR observations) as follows (Rover and Vitti 2019; Ghiasi 2020; Wang et al. 2018 and 2019; Farzaneh et al. 2021):

$$SNR^2 = A_D^2 + 2A_D A_R \cos \delta\varphi (A_D \gg A_R) \tag{1}$$

where A_D and A_R represent the amplitudes of the direct and reflected signals, respectively, and the $\delta\varphi$ component represents the phase difference between the two signals. The SNR received by the receiver can be presented in two parts. The first part is primarily attributed to the direct signal, and the second part is due to the multipath interference between the two signals (Bilich and Larson 2007). The process of estimating the height of the antenna from the reflection level was proposed in previous studies (Lowe et al. 2002; Bilich and Larson 2007). Accordingly, the reflected signal propagates an additional distance than the direct signal, which indicates the delay of this signal compared to the direct signal. For example,

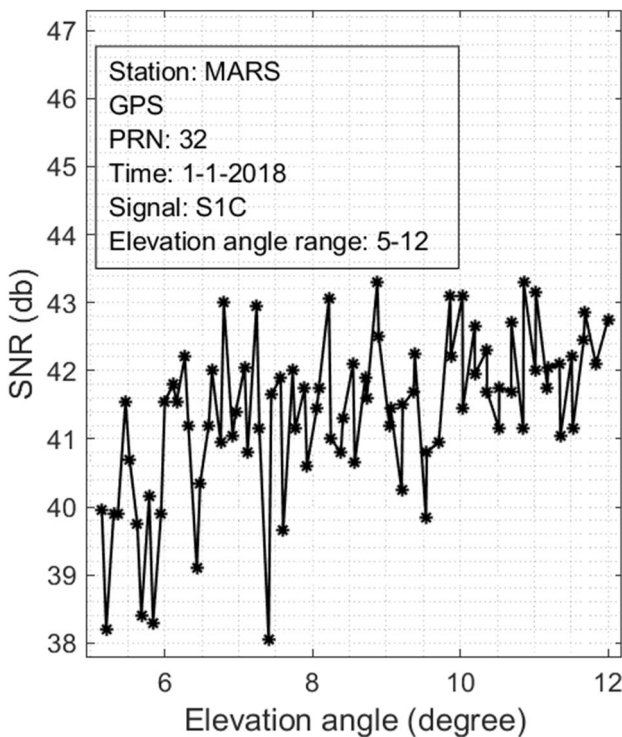


Fig. 3 SNR observations for satellite number 32 of the GPS navigation system on the first day of 2018 in the station MARS

Fig. 3 shows the SNR variations considering only S1C-GPS signal and different elevation angles at station MARS.

Based on what is shown in Fig. 4, the additional distance (AD) between two signals can be calculated as follows:

$$AD = 2H \sin(e) \tag{2}$$

In (2), e is the satellite elevation angle, AD is the additional distance between two signals, and H is the vertical distance between the antenna phase center reflecting and the surface. In the following, the phase difference between two direct and reflected signals is presented as follows (Larson and Nievinski 2013; Wang et al. 2018; Farzaneh et al. 2021):

$$\delta\varphi = 4\pi H \frac{\sin(e)}{\lambda} \tag{3}$$

where λ represents the wavelength of the GNSS signal. Therefore, considering the movement of the sea surface and the satellite, the derivative of the relative multipath phase in terms of time can be presented as follows:

$$\frac{d\delta\varphi}{dt} = 4\pi \left(\dot{H} \frac{\sin(e)}{\lambda} + H \frac{\cos(e)}{\lambda} \dot{e} \right) \tag{4}$$

where \dot{e} is the elevation angle rate and \dot{H} is the vertical velocity. In addition, Eq. (4) can be rewritten as follows:

$$\frac{d\delta\varphi}{dt} (\cos(e)\dot{e})^{-1} = 4\pi \left(\dot{H} \frac{\tan(e)}{\lambda\dot{e}} + H \frac{1}{\lambda} \right) \tag{5}$$

Equation (5) in static mode ($\dot{H} = 0$) and assuming $\tau = \sin(e(t))$ can be presented as follows:

$$\frac{d\tau}{dt} = \cos(e)\dot{e} \Rightarrow \frac{dt}{d\tau} = (\cos(e)\dot{e})^{-1} \tag{6}$$

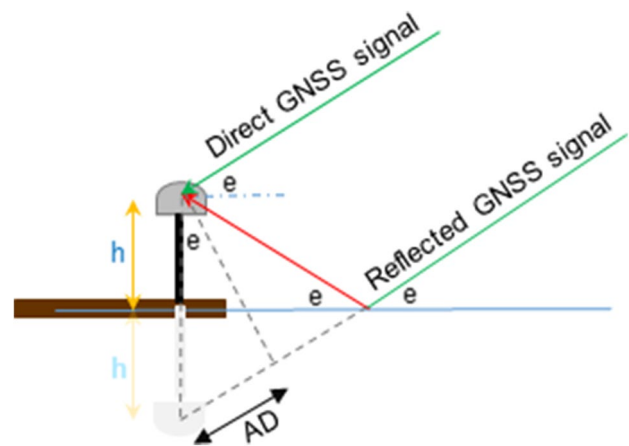


Fig. 4 A schematic illustration of GNSS-IR method for water level monitoring. Green signal: direct signal, red signal: reflected signal, e : satellite elevation angle and H : vertical distance between the antenna phase center and the reflecting surface

Therefore, by inserting (6) into (5) and considering $\frac{d\delta\varphi}{dt} = 2\pi f$ (Roussel et al. 2015; Wang et al. 2019), the relationship between frequency and phase is presented as follows:

$$H = \frac{\lambda}{2}(f_M) \quad (7)$$

where f_M is a frequency (predominant multipath frequency in SNR data) that can be calculated using various methods such as the least-square harmonic estimation (LS-HE) or Lomb–Scargle periodogram (LSP) methods. In this study, we use the LS-HE method to determine f_M (presented in supplementary materials) (Amiri-Simkooei et al. 2007; Ghiasi et al. 2020; Farzaneh et al. 2021).

Results and discussion

Today, various satellites and positioning systems such as GPS, GLONASS, Galileo, and BeiDou have been created, each capable of sending multiple signals. Therefore, it is important to verify the accuracy of each of these signals for GNSS-IR applications, e.g., sea level height (SSH) estimation. In applications such as satellite altimetry, the altitude obtained by each of these signals needs to be evaluated due to the different quality of the transmitted information. Therefore, in this study, the SSH results obtained using GNSS-IR in four GNSS stations are evaluated in the following case studies: (1) studying the SSH results obtained using GPS satellite positioning system signals, which include L1, L2 and L5, (2) studying the SSH results using GLONASS signals, including L1 and L2, (3) using Galileo satellite positioning system signals, i.e., L1, L5, L6, L7, and L8, and (4) using BeiDou signals (i.e., L2 and L7). Finally, tidal frequencies were extracted from the tide gauge and GNSS time series using the LS-HE approach, and the principal frequencies were compared.

Comparison of the SSH results using L1, L2 and L5 GPS signals

In this section, stations AT01, GTGU, MCHN, and MERS are used. The receiving stations observe the L1 and L2 signals, and the AT01 and station MERS also receive L5 signals. We evaluated the quality of GPS signals to extract the SSH using the accuracy (RMSE) and correlation coefficient using the results of GNSS-IR and coastal tide gauge observations. Table 1 presents the results of SSH estimations by employing daily and hourly data. Figures 5, 11 and 12 (presented in the appendix) show the time series (hourly) related to the signals L1, L2 and L5 and the tide gauge observations for the desired stations. The figures illustrate that the obtained sea level heights by GNSS-IR and tide gauge data

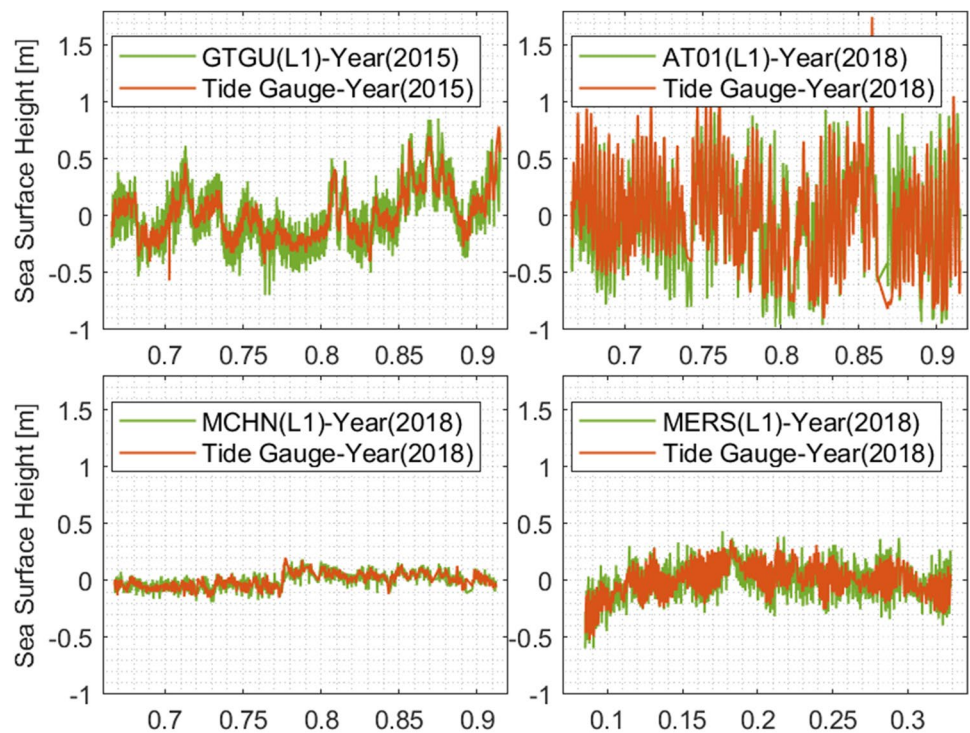
Table 1 Comparison of the obtained SSH results using hourly and daily GPS satellite signals in stations AT01, GTGU, MCHN, and MERS

Station name	Signal name	RMSE (m)	Correlation coefficient
AT01	L1 daily	0.16	0.80
	L1 hourly	0.27	0.78
	L2 daily	0.11	0.91
	L2 hourly	0.24	0.82
	L5 daily	0.12	0.89
GTGU	L5 hourly	0.26	0.77
	L1 daily	0.06	0.95
	L1 hourly	0.13	0.85
	L2 daily	0.10	0.95
	L2 hourly	0.19	0.85
MCHN	L1 daily	0.02	0.87
	L1 hourly	0.05	0.69
	L2 daily	0.13	0.09
	L2 hourly	0.15	0.12
	L5 daily	0.34	0.33
MERS	L5 hourly	1.15	0.22
	L1 daily	0.03	0.95
	L1 hourly	0.09	0.81
	L2 daily	0.38	0.21
	L2 hourly	1.11	0.22

are consistent and the time series fluctuations are similar, except for L2 and L5 signals at station MERS. Generally, the L1 GPS signal (daily) provides smaller RMSE with respect to the other signals. It is worth mentioning that the hourly and daily results are obtained by averaging all sea level heights obtained for each hour and day, respectively. However, the results depend on the number of available satellites.

As presented in Table 1, the comparison of RMSE and correlation of different signals related to each system was investigated in four stations, using hourly and daily observations over a period of three months. In hourly and daily mode, the best accuracy and the highest correlation were reported for the L1 signal except for station AT01, which shows the L2 signal is better. In addition, the results show that the observation sampling rate plays a significant role. For example, in the case of using hourly observations, the smallest RMSE for the station MCHN is obtained 5 cm. Also, for this station, the correlation coefficient is 0.69. By changing the observation sampling rate to daily, the best accuracy (the smallest RMSE) was reported for the station MCHN, with a value of 2 cm and a correlation of 0.87. The results of the station MERS show that the RMSEs using the L1 signal are 3 and 9 cm for daily and hourly observations, respectively. Also, the corresponding correlation coefficients for this station are 0.95 and 0.81. For station GTGU, the RMSE of 6 and 13 cm are estimated using daily and hourly

Fig. 5 Sea level time series obtained from hourly GPS L1 signal and coastal tide gauge at stations GTGU, AT01, MCHN, and MERS. The x-axes show decimals of the year



observations for the L1 signal. The correlation coefficients are 0.95 and 0.85. Finally, in station AT01, unlike other stations, the L2 signal has provided better results. One of the reasons could be the long distance (about 74 km) from the tide gauge station in station AT01. The L2 signal in this station has a daily and hourly RMSE of 11 and 24 cm, respectively. The correlation coefficients for this signal are 0.91 and 0.82. Also, in this station, all three L1, L2 and L5 signals show larger RMSE values than other stations. Therefore, it can be difficult to draw conclusions in station AT01 using the existing tide gauge station. In other stations, following the L1 signal, the L2 signal has produced good results in terms of smaller RMSE, and the amount of change related to the correlation coefficient is nearly comparable.

Comparison of the SSH results using L1 and L2 GLONASS signals

In this section, stations AT01, GTGU, and MERS are used to estimate the SSH and compare the obtained results using GLONASS L1 and L2 signals. The station MCHN was excluded because the mounted receiver in this station cannot track the GLONASS signals. The accuracy (RMSE) and correlation coefficient between the obtained SSH using GNSS-IR and coastal tide observations are shown in Table 2. Figures 6 and 13 (presented in the appendix) show the time series related to the L1 and L2 signals and the tide gauge observations. Similarly, by comparing the GNSS-IR and tide gauge results, one can observe that the daily observations

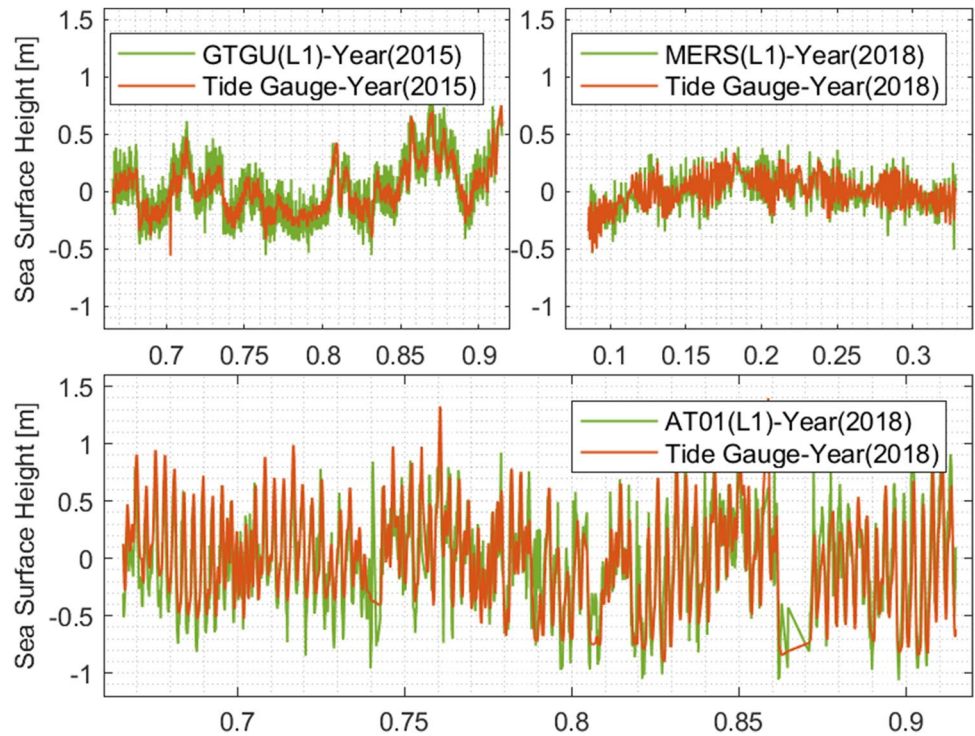
Table 2 Comparison of SSH results using hourly and daily GLO-NASS satellite signals in stations AT01, GTGU, and MERS

Station name	Signal name	RMSE (m)	Correlation coefficient
AT01	L1 daily	0.15	0.85
	L1 hourly	0.27	0.77
	L2 daily	0.12	0.90
GTGU	L2 hourly	0.24	0.82
	L1 daily	0.06	0.96
	L1 hourly	0.13	0.86
	L2 daily	0.10	0.96
MERS	L2 hourly	0.19	0.86
	L1 daily	0.04	0.91
	L1 hourly	0.09	0.82
	L2 daily	0.52	0.20
	L2 hourly	1.03	0.03

provided better results than hourly observations. Generally, the results show that the time series and fluctuations are similar, except for the L2 signal at station MERS.

The results presented in Table 2 show that the GLO-NASS L1 signal (daily observations) provided better results because of smaller RMSE and higher correlation coefficient values. The L1 signal of the station MERS shows the lowest RMSE value in daily mode, which is equal to 4 cm, and the correlation coefficient is 0.91. The RMSE using the same signal is 9 cm (in the hourly mode), giving a correlation

Fig. 6 Sea level time series obtained from the hourly GLO-NASS L1 signal and coastal tide gauge in stations GTGU, MERS and AT01. The x-axes show decimals of the year



coefficient of 0.82. For station GTGU, values of 6 and 13 cm are obtained for RMSE in daily and hourly mode, and the correlation coefficients are 0.96 and 0.86, respectively. Finally, in station AT01, unlike other stations, the obtained RMSEs using L2 signal are 12 and 24 cm considering daily and hourly modes, respectively, and the correlation coefficients are 0.90 and 0.82, respectively.

In general, it can be concluded that the L1 signal provides more accurate results than the L2 signal, but in the case of the station AT01, the accuracy of the L2 signal is better than the L1 signal.

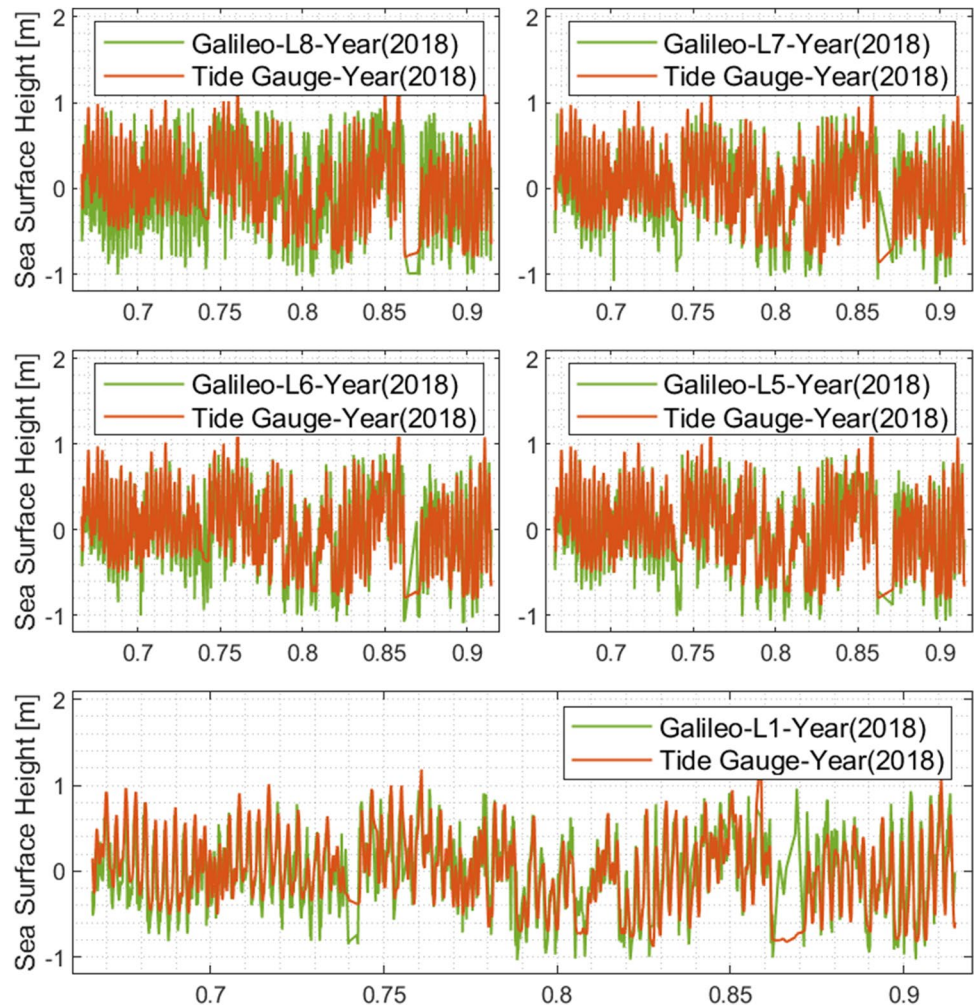
Comparison of the SSH results using L1, L5, L6, L7 and L8 Galileo signals

We analyzed the discrepancies between the SSH values obtained by GNSS-IR and tide gauge data using Galileo signals in this section. For this purpose, we used only stations AT01 and MERS in this section because they can track the Galileo signals. The station AT01 is able to receive five signals, i.e., L1, L5, L6, L7 and L8, and station MERS receives L1, L5, L7 and L8 signals. Similarly, the results are shown in Table 3. These comparisons are presented using the different observation sampling rates, i.e., daily and hourly modes for the desired signals.

Table 3 Comparison of SSH results using hourly and daily Galileo satellite signals in stations AT01 and MERS

Station name	Signal name	RMSE (m)	Correlation coefficient
AT01	L1 daily	0.23	0.63
	L1 hourly	0.29	0.74
	L5 daily	0.12	0.89
	L5 hourly	0.26	0.79
	L6 daily	0.11	0.91
	L6 hourly	0.26	0.80
	L7 daily	0.14	0.85
	L7 hourly	0.26	0.79
	L8 daily	0.18	0.78
MERS	L8 hourly	0.36	0.63
	L1 daily	0.04	0.88
	L1 hourly	0.08	0.83
	L5 daily	0.78	0.19
	L5 hourly	1.33	0.17
	L7 daily	0.77	0.12
	L7 hourly	1.30	0.20
	L8 daily	0.78	0.20
L8 hourly	1.33	0.20	

Fig. 7 Sea level time series obtained from the hourly Galileo L1, L5, L6, L7 and L8 signals and coastal tide gauge in station AT01. The x-axes show decimals of the year



Figures 7 and 14 (presented in the appendix) show the time series of the estimated SSH and the tide gauge observations in stations AT01 and MERS. Generally, as can be seen in Figs. 7 and 14, the results show that the time series and fluctuations are similar (except for station MERS and using the L1 signal). Similarly, the daily observations provided smaller RMSE with respect to tide gauge data because daily averaging can filter out existing errors.

According to Table 3, the Galileo L1 signal provides more accurate data than the other signals at the station MERS. The results show a value of 4 and 8 cm for RMSE in daily and hourly modes, respectively, and corresponding correlation coefficients of 0.88 and 0.83. In the following, for station AT01, the L6 signal has been obtained with a value of 11 and 26 cm for RMSE using daily and hourly observations. Also, the corresponding correlation coefficients are 0.91 and 0.80. In station AT01, after the L6 signal, the L5 signal showed the best accuracy, but in station MERS, the other signals provided similar results.

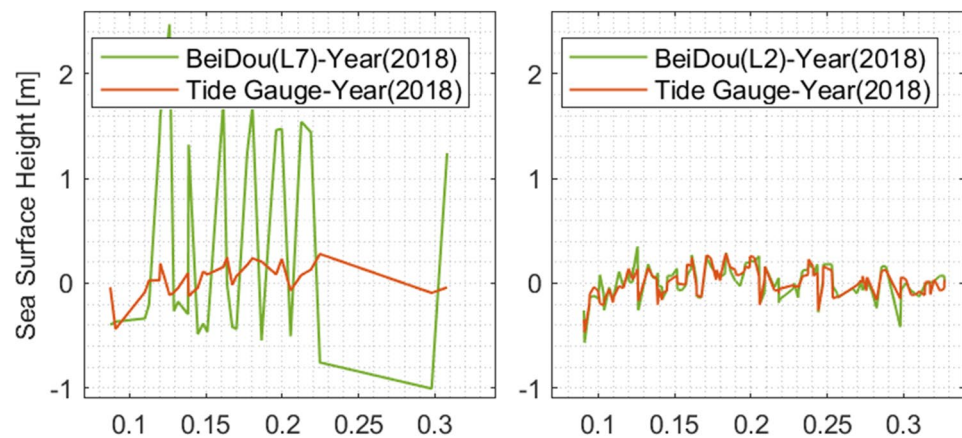
Table 4 Comparison of BeiDou satellite signal results in station MERS

Station Name	Signal name	RMSE (m)	Correlation coefficient
MERS	L2 daily	0.12	0.52
	L2 hourly	0.08	0.83
	L7 daily	0.98	0.15
	L7 hourly	1.02	0.12

A comparison of the SSH results using L2 and L7 BeiDou signals

This section uses only the collected data at the station MERS because it can track the BeiDou L2 and L7 signals. The RMSE and correlation coefficient between the obtained SSH using BeiDou data and tide observations are presented in Table 4 and Fig. 8. These comparisons are presented in both daily and hourly results for L2 and L7 signals. Figure 8

Fig. 8 Sea level time series obtained from the hourly BeiDou L2 and L7 signals and coastal tide gauge in station MERS. The x-axis shows decimals of the year



shows that the L7 signal provides more significant discrepancies than the L2 signal.

Based on what is presented in Table 4, the best BeiDou satellite signal at the station MERS is the L2 signal with an RMSE 8 cm and 12 cm for hourly and daily observation rates, respectively. Also, the corresponding correlation coefficients are 0.83 and 0.52.

The study of frequencies extracted from reflectometry and tide gauge time series is an important and independent criterion for analyzing the obtained two-time series. For this purpose, after selecting the best signal from GPS, Galileo, GLONASS and BeiDou systems (i.e., GPS L1), the frequencies extracted from two-time series of reflectometry and tide gauge are examined and compared. In the next section, we show the results of the frequency analysis.

Tidal frequencies extraction using spectral analysis

One of the main goals of this research is to compare the tidal components obtained from GNSS-IR and tide gauge data. This study can quantify how good the GNSS-IR method is for tide studies. To do this, we use power spectral density (PSD) estimation using the univariate LS-HE method to compare GNSS-IR and tide gauge time series. Then, using univariate analysis (LSHE), the tidal frequencies are extracted (see supplementary materials). In other words, using LS-HE, one can extract all frequencies in the data. It is also worth mentioning that, although sea level data are time-dependent, different types of noises, like random walk and flicker noises (color noises), should be considered. However, other methods, like the Fourier spectral analysis method, can be applied for the time series with zero mean value, white noise and identical interval. Therefore, a proper method for spectral harmonic analysis, such as the LSHE, should be considered. The GNSS-IR time series of the station MARS in France, the station TGDE in Norway, and the two nearby tide gauge stations, MARSEILLE and TREGDE, are used for this purpose. Using the univariate analysis method,

the power spectrum of the time series is calculated for the GNSS-IR and tide gauge time series. The results are shown in Fig. 9 for stations MARS and TGDE, respectively.

The dominating frequencies in the desired time series were recovered using the LSHE approach and the results are visualized in Fig. 9. The results show that both time series from the GNSS-IR and tide gauge have primary frequency values that are in reasonable agreement. The GNSS-IR approach can be utilized as a viable tool for tide modeling in coastal locations because these frequencies are crucial for signal modeling and sea surface change prediction. The results pertaining to these primary components are shown in Figs. 10, 15, 16 and 17 (presented in the appendix), considering that roughly 90% of signals are created using daily, semi-daily, and hourly frequencies. The details of the main astronomical frequencies, which are also included in the list of 145 main astronomical frequencies, are presented in Table 5.

Figures 10, 15, 16, and 17 (see also the appendix) illustrate two instances by utilizing the tide station's time series and the time series acquired using the GNSS-IR approach. The figures confirm a reasonable agreement for the major tidal component in the tide gauge and GNSS-IR data. This means that it is possible to obtain the main tide frequencies, such as diurnal and semidiurnal frequencies, using the time series of GNSS observations, and these results are in good agreement with the presented astronomical frequencies. Based on these findings, it can be concluded that the GNSS-IR data can be employed for additional marine applications, such as tidal modeling and tide prediction, in addition to achieving water level changes. The frequencies obtained from the reflectometry time series have an acceptable degree of proximity compared to the extracted frequencies of the tide gauge time series analysis, which provides the water level elevation with the highest accuracy. Moreover, the tide gauge station records the most accurate observations for the instantaneous water level, but the reflectometry method with fewer constraints obtained these components with a high correlation coefficient. In the following, the frequencies

Fig. 9 Univariate least-squares power spectrum of four time series provided from Tide gauges and GNSS-IR stations. (Top left) Power spectrum for station MARS time series obtained from GNSS-IR. (Top right) Power spectrum for station MARS time series obtained from Tide gauge. (Bottom left) Power spectrum for station TGDE time series obtained from GNSS-IR. (bottom right) Power spectrum for station TGDE time series obtained from Tide gauge. The *x*-axes show period in hour

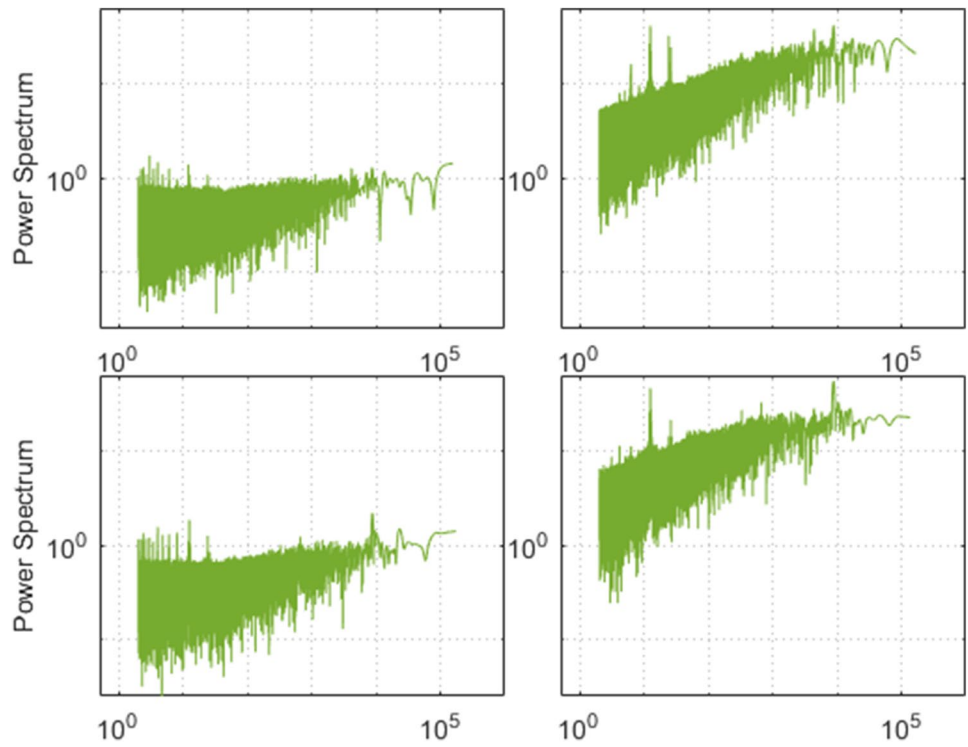


Fig. 10 Semidiurnal and diurnal signals in the univariate power spectrum obtained from GNSS-IR observations of the station MARS. The *x*-axes show period in hour

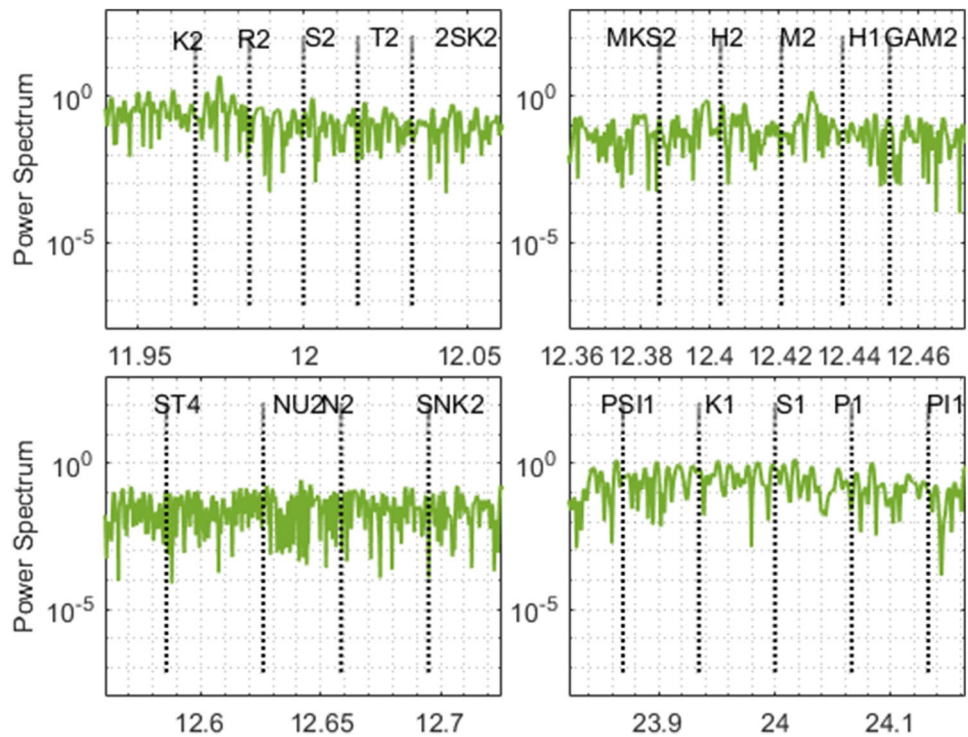


Table 5 Characteristics of the 19 main astronomical frequencies (<https://tidesandcurrents.noaa.gov>)

No	Tidal component	Period (hours)
1	K2 Lunisolar semidiurnal constituent	11.967235
2	R2 Smaller solar elliptic constituent	11.983596
3	S2 Principal solar semidiurnal constituent	12.000000
4	T2 Larger solar elliptic constituent	12.016449
5	2SK2	12.032945
6	ST4	12.585651
7	NU2 Larger lunar evectional constituent	12.626004
8	N2 Larger lunar elliptic semidiurnal constituent	12.658348
9	SNK2	12.695013
10	MKS2	12.385502
11	H2	12.403028
12	M2 Principal lunar semidiurnal constituent	12.420601
13	H1	12.438225
14	GAM2	12.451900
15	PSI1	23.869299
16	K1 Lunar diurnal constituent	23.934470
17	S1 Solar diurnal constituent	23.999997
18	P1 Solar diurnal constituent	24.065890
19	PI1	24.132140

extracted from the reflectometer and tide gauge time series related to 145 astronomical frequencies in Tables S3 to S6 are presented (presented in supplementary materials).

Conclusion

GNSS multipath error is one of the most significant sources of inaccuracy in obtaining high-accuracy positioning. Studies have revealed that this kind of error offers helpful information for various applications over time. One of these applications is calculating sea surface changes using GNSS multipath signal. High temporal and spatial resolution measurements of sea level altitude can be made using GNSS signals that are reflected from the water sea level. The purpose of this study was to calculate the sea level height using the GNSS-IR technique and to compare the results obtained from different signals of GPS, GLONASS, Galileo, and BeiDou with coastal tide observations. In addition, we used the Least Square Harmonic Estimation (LS-HE) approach, which allows for extracting the tidal frequencies

from both the GNSS-IR and tide gauge data. For this purpose, data from six stations were used in this study, i.e., AT01 (Alaska), GTGU (Sweden), MCHN (Canada), MERS (Turkey), MARS (France), and TGDE (Norway). Our results showed that the sea level height measured by the L1 signal of GPS satellite provides a better and more accurate solution than other systems. For example, the RMSE and correlation coefficients are: in station MCHN with an accuracy of 2 cm and a correlation of 0.95, in station MERS with an accuracy of 3 cm and a correlation of 0.87, and station GTGU with an accuracy of 6 cm and a correlation of 0.95. In addition, the L1 signal of GPS satellite provided better results compared to the L2 and L5 signals. At station AT01, the L2 signal, with an accuracy of 11 cm, was more correlated with the tide gauge observation than the L1 signal, with an accuracy of 16 cm. In relation to the GLONASS satellite positioning system, whose L1 and L2 signals have been used in 3 stations, L1 in station GTGU, with 4 cm accuracy and a correlation coefficient of 0.91, presented the best results compared to other signals. The results of evaluating the Galileo signals, i.e., L1, L5, L6, L7 and L8 at the two stations AT01 and MERS, indicated that the L1 and L6 signals provide the best results compared to other signals. The L1 signal showed an accuracy of 4 cm and a correlation of 0.88 at the station MERS, and the L6 signal an 11 cm RMSE and a 0.91 correlation coefficient at the station AT01. Among the studied stations, only MERS detects the BeiDou satellite, which includes two signals, L2 and L7. The comparisons at this station showed that the L2 signal, with an accuracy of 8 cm and a correlation of 0.83, offers better results than the L7 signal.

Finally, the tidal frequencies obtained from the sea level height, using the GPS L1 signal, were extracted at stations MARS and TGDE. We used the LS-HE method for this purpose. The results showed that the tidal frequencies can be estimated with high accuracy using GNSS-IR technique. The correlation coefficients are 0.99 and 1.00 compared to the tidal frequencies extracted from the time series of nearby coastal tide gauges. The results confirmed that the GNSS-IR can be used for tide modeling studies, especially in areas with no tide gauge data.

Appendix

See Figs. 11, 12, 13, 14, 15, 16 and 17.

Fig. 11 Sea level time series obtained from hourly GPS L2 signal and coastal tide gauge in stations GTGU, AT01, MCHN, and MERS. The x-axes show decimals of the year

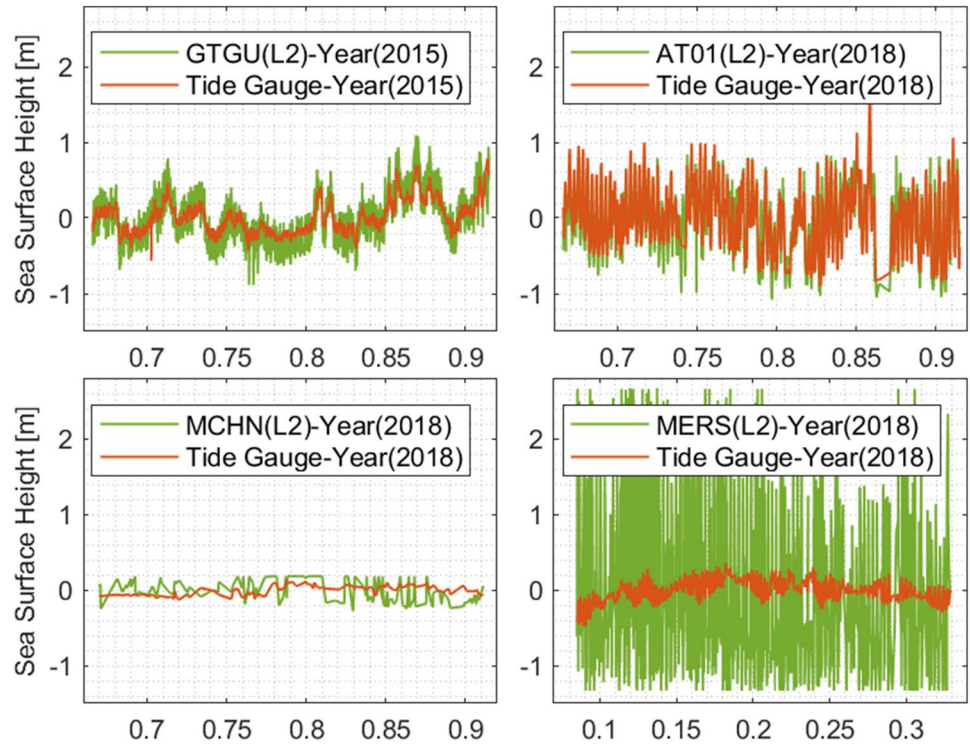


Fig. 12 Sea level time series obtained from hourly GPS L5 signal and coastal tide gauge in stations AT01 and MERS. The x-axes show decimals of the year

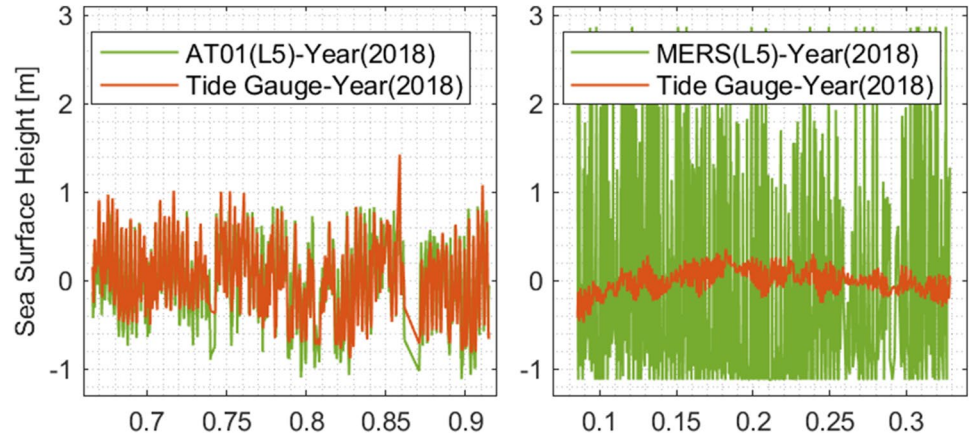


Fig. 13 Sea level time series obtained from the hourly GLO-NASS L2 signal and coastal tide gauge in stations GTGU, MERS and AT01. The *x*-axes show decimals of the year

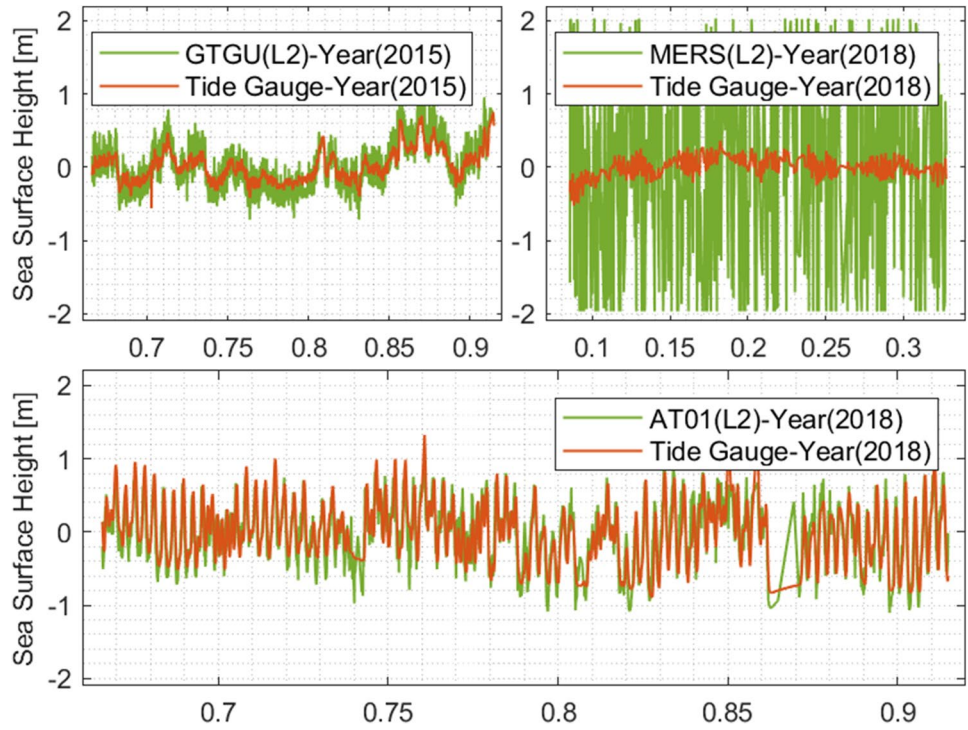


Fig. 14 Sea level time series obtained from the hourly Galileo's L1, L5, L7 and L8 signals and coastal tide gauge in station MERS. The *x*-axes show decimals of the year

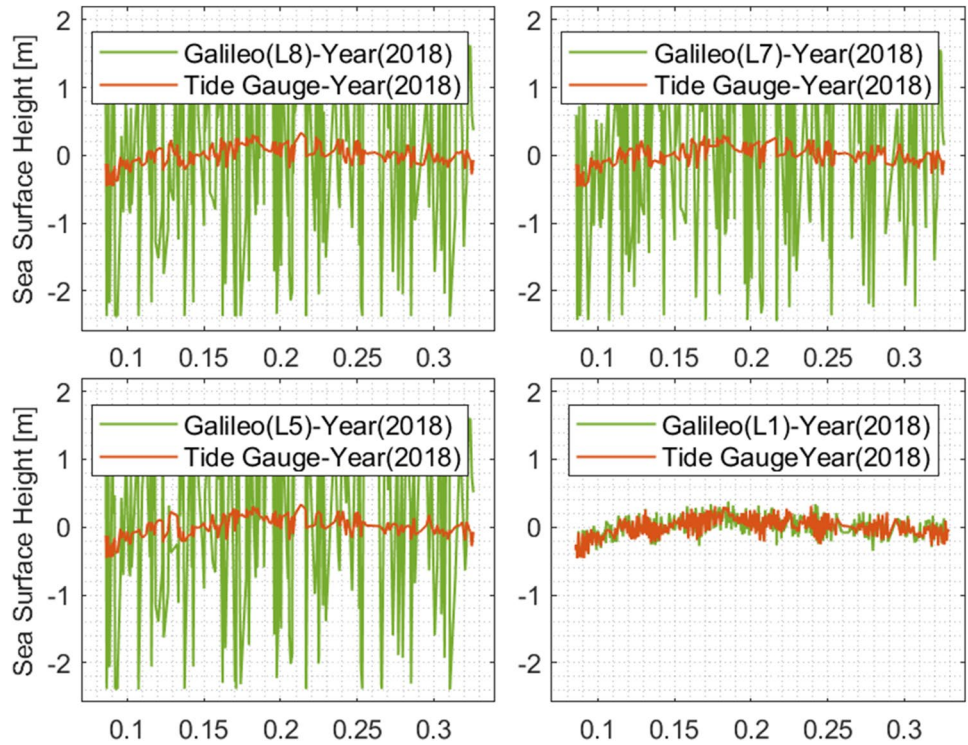


Fig. 15 Semidiurnal and diurnal signals in the univariate power spectrum obtained from tide gauge observations of the station MARS. The *x*-axes show period in hour

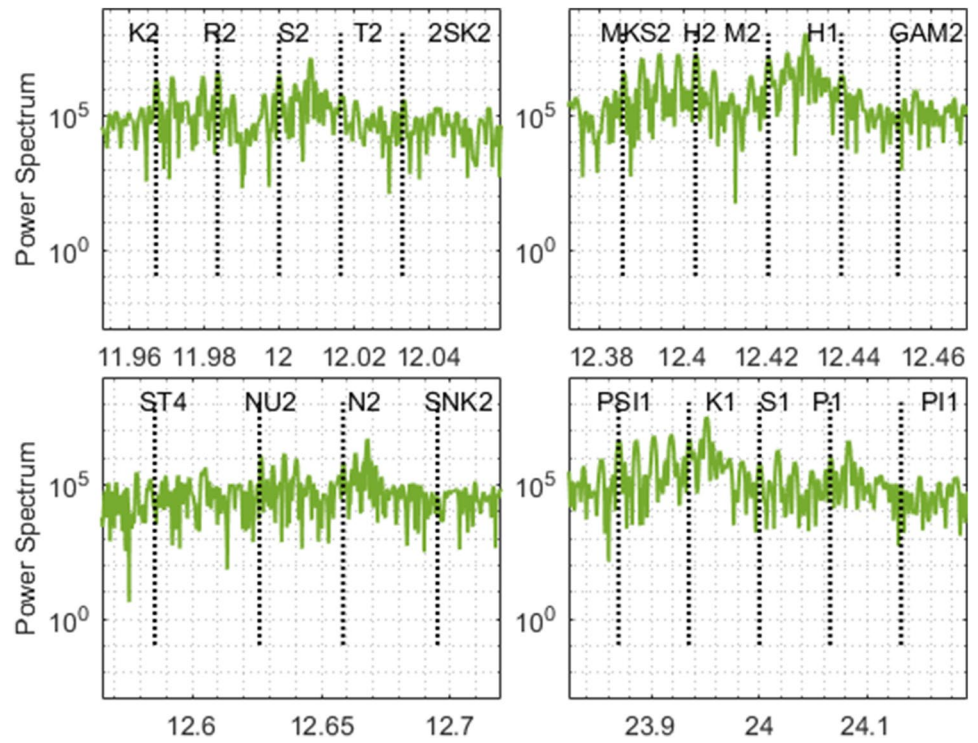


Fig. 16 Semidiurnal and diurnal signals in the univariate power spectrum obtained from GNSS-IR observations of the station TGDE. The *x*-axes show period in hour

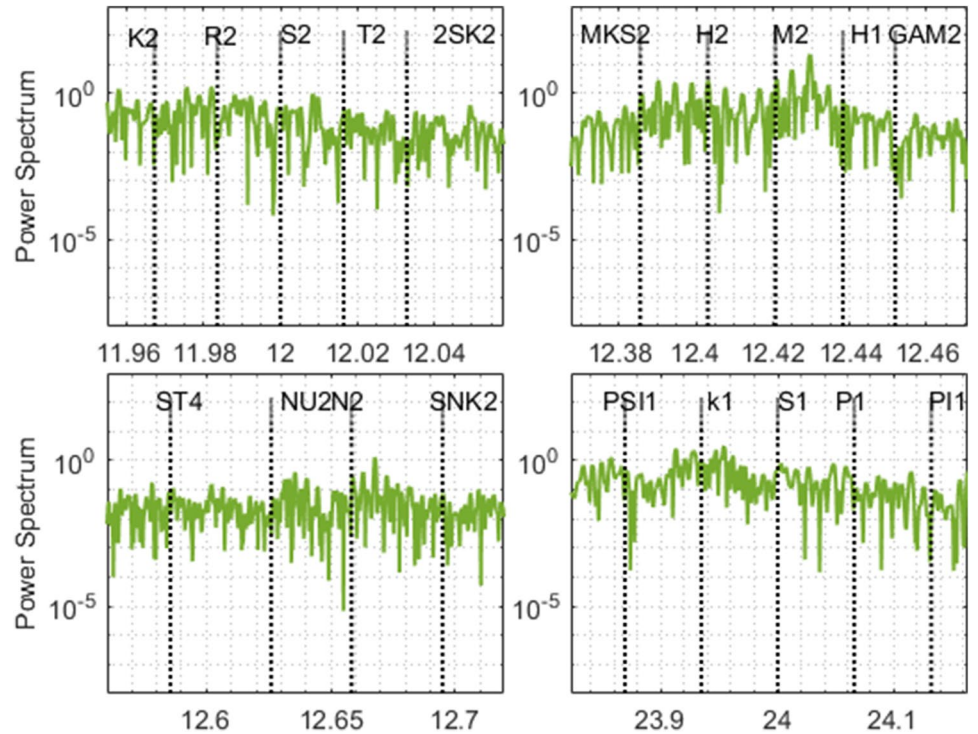
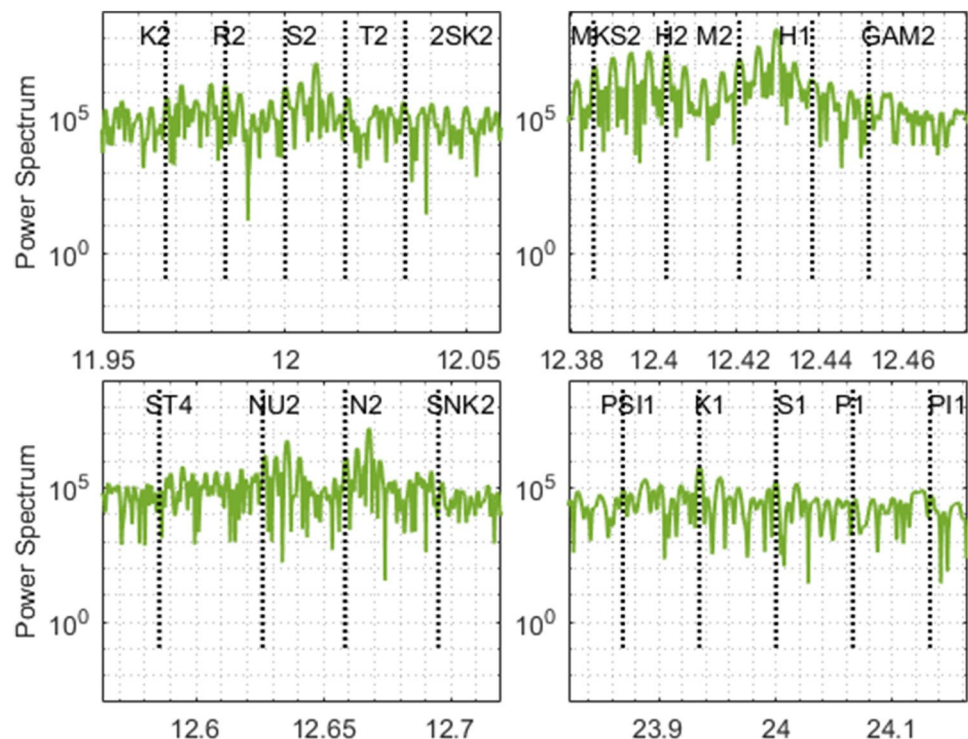


Fig. 17 Semidiurnal and diurnal signals in the univariate power spectrum obtained from tide gauge observations of the station TGDE. The x -axes show period in hour



Supplementary Information The online version contains supplementary material available at <https://doi.org/10.1007/s10291-023-01416-6>.

Acknowledgements The authors are going to thank the IGS and PSMSL for providing the RINEX data and tide gauge water level data. We thank the editor-in-chief and anonymous reviewers for their careful reading of our manuscript and their many insightful comments and suggestions.

Author contributions SG contributed to coding, test on real data, writing, and investigation. MB contributed to supervision, discussions and suggestions during the development, and methodology. KP provided the main conceptual ideas and contributed to the writing, investigation, coding, advising, and conceptual development. SF contributed to writing, the coding, investigation, designing, supervision and conceptual development.

Data availability All the data used in this research were obtained from publicly available data sources. The RINEX GNSS observation files can be downloaded from <http://www.igs.org>. Files related to time series of water level observations for tide-gauge stations can be downloaded from <http://www.psmsl.org>.

Declarations

Competing interests The authors declare no competing interests.

References

Amiri-Simkooei AR, Tiberius CC, Teunissen PJ (2007) Assessment of noise in GPS coordinate time series: methodology and results. *J Geophys Res Solid Earth* 112(B7):B07413

- Benton CJ, Mitchell CN (2011) Isolating the multipath component in GNSS signal-to-noise data and locating reflecting objects. *Radio Sci* 46(06):1–11
- Bilich A, Larson KM (2007) Correction published 29 March 2008: mapping the GPS multipath environment using the signal-to-noise ratio (SNR). *Radio Sci* 42(06):1–16
- Castagnetti C, Casula G, Dubbini M, Capra C (2009) Adjustment and transformation strategies of ItalPoS permanent GNSS network. *Ann Geophys* 52(2):181–185
- Cohen JE, Small C, Mellinger A, Gallup J, Sachs J (1997) Estimates of coastal populations. *Science* 278(5341):1209–1213
- Farzaneh S, Parvazi K (2020) Noise analysis of satellites altimetry observations for improving chart datum within the Persian Gulf and Oman Sea. *Ann Geophys* 62(5):558
- Farzaneh S, Parvazi K, Shali HH (2021) GNSS-IR-UT: A MATLAB-based software for SNR-based GNSS interferometric reflectometry (GNSS-IR) analysis. *Earth Sci Inf* 14(3):1633–1645
- Feng G, Jin S, Zhang T (2013) Coastal sea level changes in Europe from GPS, tide gauge, satellite altimetry and GRACE, 1993–2011. *Adv Space Res* 51(6):1019–1028
- Ghiasi SY (2020) Application of GNSS interferometric reflectometry for lake ice studies. Master's thesis, University of Waterloo
- Ghiasi Y, Duguay CR, Murfit J, van der Sanden JJ, Thompson A, Drouin H, Prevost C (2020) Application of GNSS interferometric reflectometry for the estimation of lake ice thickness. *Remote Sens* 12(17):2721
- Larson KM, Nievinski FG (2013) GPS snow sensing: results from the earthscope plate boundary observatory. *GPS Solutions* 17(1):41–52
- Larson KM, Löfgren JS, Haas R (2013) Coastal sea level measurements using a single geodetic GPS receiver. *Adv Space Res* 51(8):1301–1310
- Larson KM, Ray RD, Williams SD (2017) A 10-year comparison of water levels measured with a geodetic GPS receiver versus a conventional tide gauge. *J Atmos Ocean Tech* 34(2):295–307

- Löfgren JS, Haas R, Scherneck HG (2014) Sea level time series and ocean tide analysis from multipath signals at five GPS sites in different parts of the world. *J Geodyn* 80:66–80
- Lowe ST, Zuffada C, Chao Y, Kroger P, Young LE, LaBrecque JL (2002) 5-Cm-Precision aircraft ocean altimetry using GPS reflections. *Geophys Res Lett* 29(10):1375
- Martin-Neira M (1993) A passive reflectometry and interferometry system (PARIS): application to ocean altimetry. *ESA J* 17(4):331–355
- Nievinski FG, Larson KM (2014) Forward modeling of GPS multipath for near-surface reflectometry and positioning applications. *GPS Solut* 18(2):309–322
- Olivieri M, Spada G (2016) Spatial sea-level reconstruction in the Baltic Sea and in the Pacific Ocean from tide gauges' observations. *Ann Geophys* 59(3):323
- Pajak K, Kowalczyk K (2019) A comparison of seasonal variations of sea level in the southern Baltic Sea from altimetry and tide gauge data. *Adv Space Res* 63(5):1768–1780
- Peng D, Hill EM, Li L, Switzer AD, Larson KM (2019) Application of GNSS interferometric reflectometry for detecting storm surges. *GPS Solutions* 23(2):1–11
- Roussel N, Ramillien G, Frappart F, Darrozes J, Gay A, Biancale R, Striebig N, Hanquiez V, Bertin X, Allain D (2015) Sea level monitoring and sea state estimate using a single geodetic receiver. *Remote Sens Environ* 171:261–277
- Rover S, Vitti A (2019) GNSS-R with low-cost receivers for retrieval of antenna height from snow surfaces using single-frequency observations. *Sensors* 19(24):5536
- Strandberg J, Hobiger T, Haas R (2016) Inverse modelling of GNSS multipath for sea level measurements-initial results. In: 2016 IEEE international geoscience and remote sensing symposium (IGARSS). IEEE, pp 1867–1869
- Vestøl O (2006) Determination of postglacial land uplift in Fennoscandia from leveling, tide-gauges and continuous GPS stations using least squares collocation. *J Geodesy* 80(5):248–258
- Vignudelli S, Kostianoy AG, Cipollini P, Benveniste J (2011) Coastal altimetry. Springer Science & Business Media, Berlin
- Vignudelli S, Birol F, Benveniste J, Fu LL, Picot N, Raynal M, Roinard H (2019) Satellite altimetry measurements of sea level in the coastal zone. *Surv Geophys* 40(6):1319–1349
- Wang X, Zhang Q, Zhang S (2018) Water levels measured with SNR using wavelet decomposition and Lomb–Scargle periodogram. *GPS Solutions* 22(1):1–10
- Wang X, Zhang Q, Zhang S (2019) Sea level estimation from SNR data of geodetic receivers using wavelet analysis. *GPS Solutions* 23(1):1–14
- Zhang S, Liu K, Liu Q, Zhang C, Zhang Q, Nan Y (2019) Tide variation monitoring based improved GNSS-MR by empirical mode decomposition. *Adv Space Res* 63(10):3333–3345

Publisher's Note Springer Nature remains neutral with regard to jurisdictional claims in published maps and institutional affiliations.

Springer Nature or its licensor (e.g. a society or other partner) holds exclusive rights to this article under a publishing agreement with the author(s) or other rightsholder(s); author self-archiving of the accepted manuscript version of this article is solely governed by the terms of such publishing agreement and applicable law.



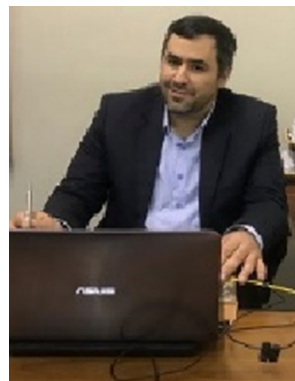
Sara Gholamrezaee is currently pursuing a master's degree in Geodesy at the University of Tehran, Iran. Her research interests include GNSS Reflectometry.



Mohammad Bagherbandi is a Professor at the University of Gävle, Sweden, and a senior researcher at the Royal Institute of Technology (KTH), Stockholm, Sweden. His professional interests include geodetic surveying, precise positioning, satellite geodesy, earth observation using satellite sensors, physical geodesy, and geodynamics. He received his PhD in Geodesy from KTH in 2011 and became an instructor (Docent) at KTH in 2013. His background is in Land Surveying Engineering. He is currently pursuing multidisciplinary research combining directions such as Geophysics, Geodesy and Land Surveying (applied geodesy).



Kamal Parvazi He received his M.Sc. degree in 2015 from the Geodesy department at the University of Isfahan, Isfahan, Iran, and his PhD degree in Geodesy at the University of Tehran in 2022. His research focused on GNSS positioning techniques with an emphasis on Precise Point Positioning (PPP). His research interests are PPP-GNSS Positioning, GNSS-Reflectometry, and Hydrography studies



Saeed Farzaneh received his M.Sc. degree in Geodesy from the University of Tehran in 2009 and a PhD in Geodesy from the University of Tehran, Iran in 2015. He is now an associate professor in the faculty of the School of Surveying and Geospatial Engineering, the University of Tehran. His research focuses on atmospheric modeling, satellite geodesy, and GNSS positioning